Designing Flexible Quantum Spin Hall Insulators through 2D Ordered Hybrid Transition Metal Carbides

Zhongheng Fu,[1,2] Zhaorui Liu,[1,2] Dominik Legut,[3] Timothy C. Germann,[4] Chen Si,[1,2] Shiyu Du,[5] Joseph S. Francisco,[6] and Ruifeng Zhang[1,2,]*

[1]School of Materials Science and Engineering, Beihang University, Beijing 100191, P. R. China

[2]Center for Integrated Computational Materials Engineering (International Research Institute for Multidisciplinary Science) and Key Laboratory of High-Temperature Structural Materials & Coatings Technology (Ministry of Industry and Information Technology), Beihang University, Beijing 100191, P. R. China

[3]IT4Innovations, VSB-Technical University of Ostrava, CZ-70800 Ostrava, Czech Republic

[4]Theoretical Division, Los Alamos National Laboratory, Los Alamos, New Mexico, 87545, United States

[5]Engineering Laboratory of Specialty Fibers and Nuclear Energy Materials, Ningbo Institute of Materials Technology and Engineering, Chinese Academy of Sciences, Ningbo, Zhejiang, 315201, P. R. China

[6]*Department of Earth and Environmental Science and Department of Chemistry, University of Pennsylvania, Philadelphia, PA, 19104, United States*

Table S1. Total energies in eV/atom of $M''_2M'C_2O_2$ in different configurations. The total energies of the most stable configurations are set as zero energy.

	configuration I	configuration II	configuration III
$Mo_2TiC_2O_2$	0.17	0.00	0.09
$W_2TiC_2O_2$	0.18	0.00	0.10
$Mo_2ZrC_2O_2$	0.14	0.00	0.07
$W_2ZrC_2O_2$	0.14	0.00	0.08
$Mo_2HfC_2O_2$	0.15	0.00	0.08
$W_2HfC_2O_2$	0.16	0.00	0.09

Table S2. Band gaps in eV of selected $M''_2M'C_2O_2$ for the test of U values of GGA + U. Note that the SOC interaction is considered in the related calculations.

U (eV)	$Mo_2TiC_2O_2$	$W_2HfC_2O_2$
0	0.04	0.28
1	0.05	0.29
2	0.06	0.31
3	0.08	0.34
4	0.11	0.38
5	0.15	0.45

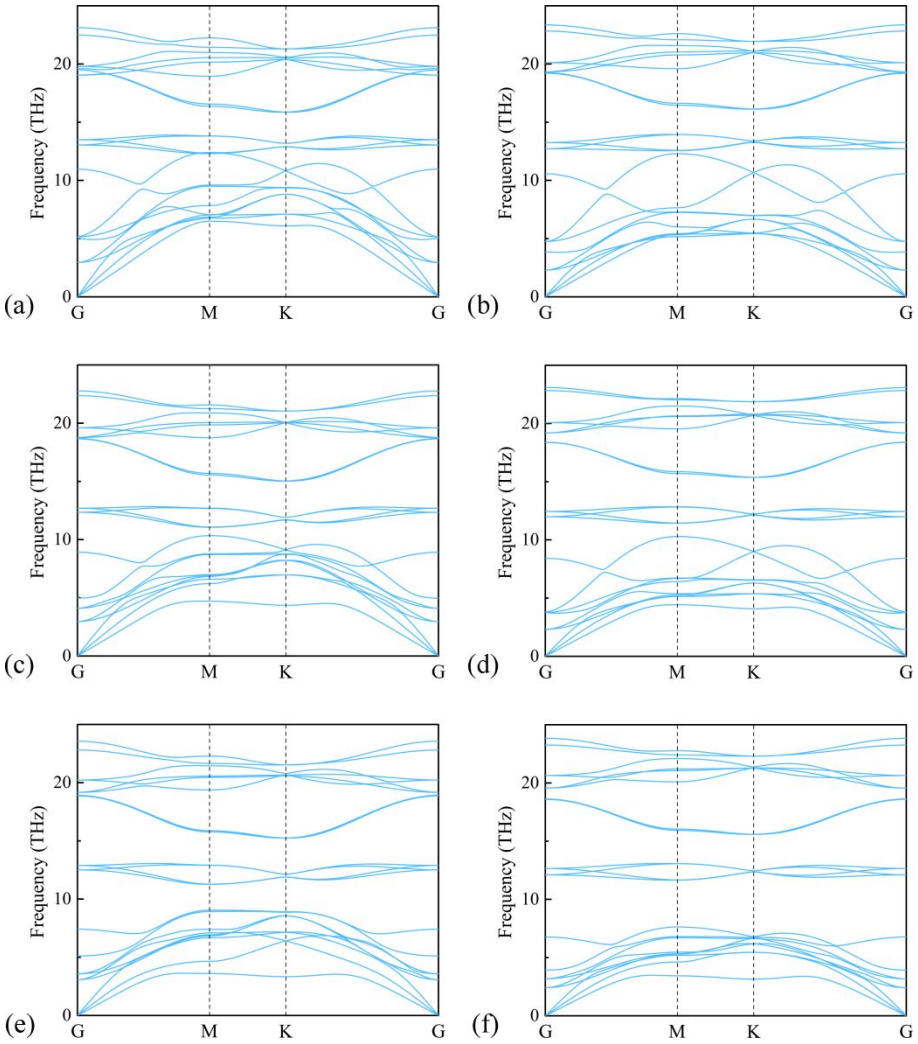

Figure S1. Phonon dispersions of (a) $Mo_2TiC_2O_2$, (b) $W_2TiC_2O_2$, (c) $Mo_2ZrC_2O_2$, (d) $W_2ZrC_2O_2$, (e) $Mo_2HfC_2O_2$, and (f) $W_2HfC_2O_2$.

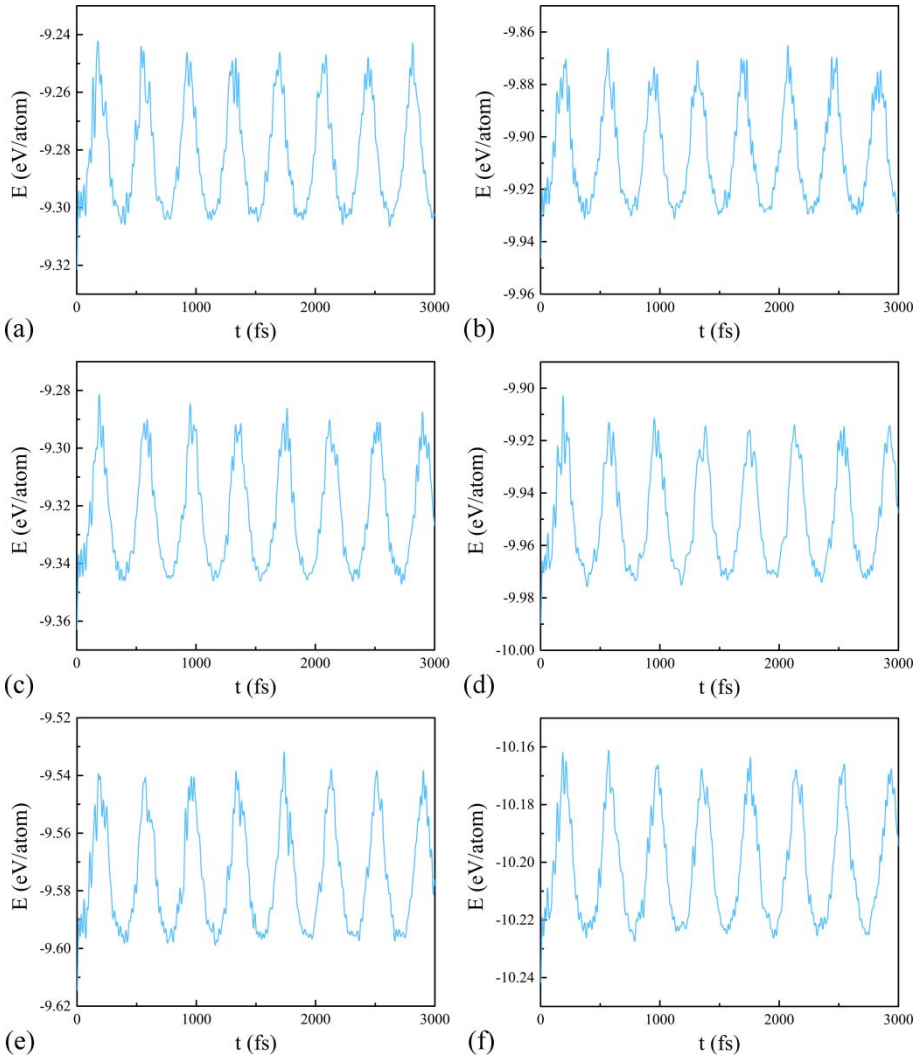

Figure S2. Variation of total energy during AIMD simulation at 300 K for (a) $Mo_2TiC_2O_2$, (b) $W_2TiC_2O_2$, (c) $Mo_2ZrC_2O_2$, (d) $W_2ZrC_2O_2$, (e) $Mo_2HfC_2O_2$, and (f) $W_2HfC_2O_2$.

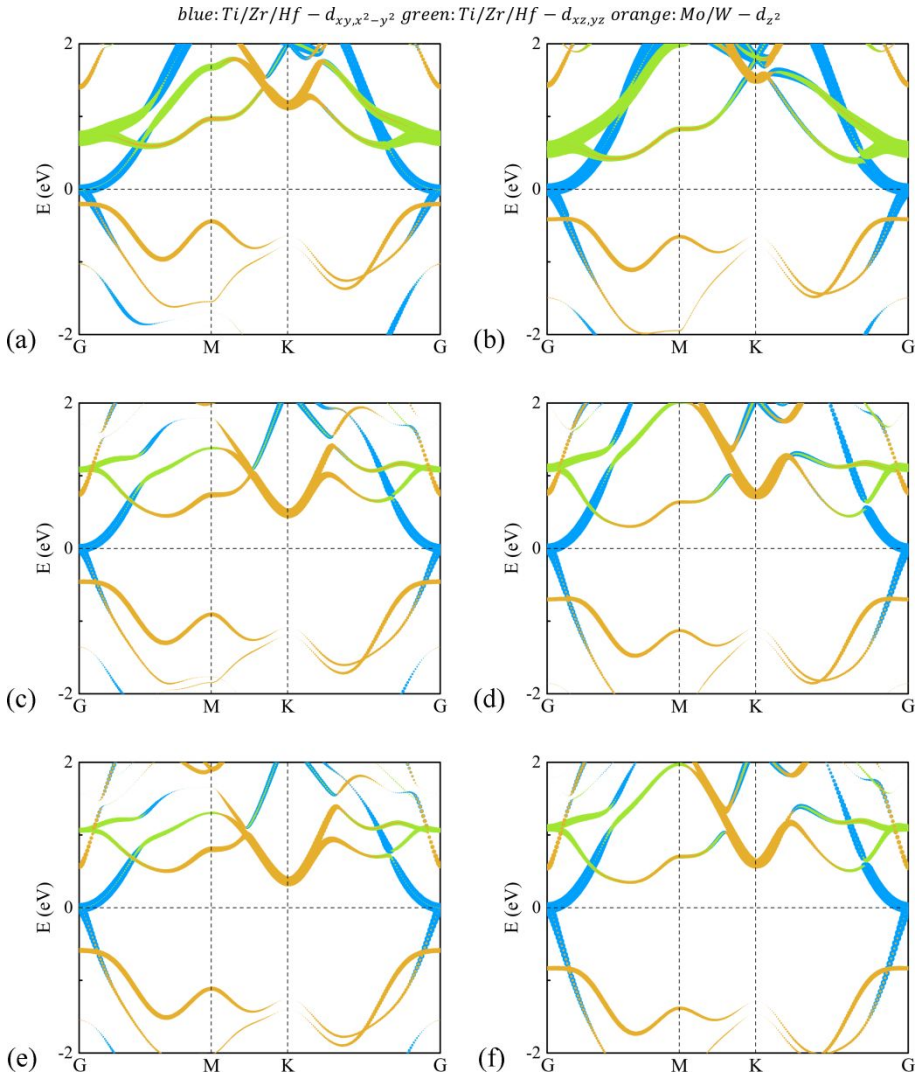

Figure S3. Projected band structures of (a) $Mo_2TiC_2O_2$, (b) $W_2TiC_2O_2$, (c) $Mo_2ZrC_2O_2$, (d) $W_2ZrC_2O_2$, (e) $Mo_2HfC_2O_2$, and (f) $W_2HfC_2O_2$ in GGA. The Fermi level is set to zero energy.

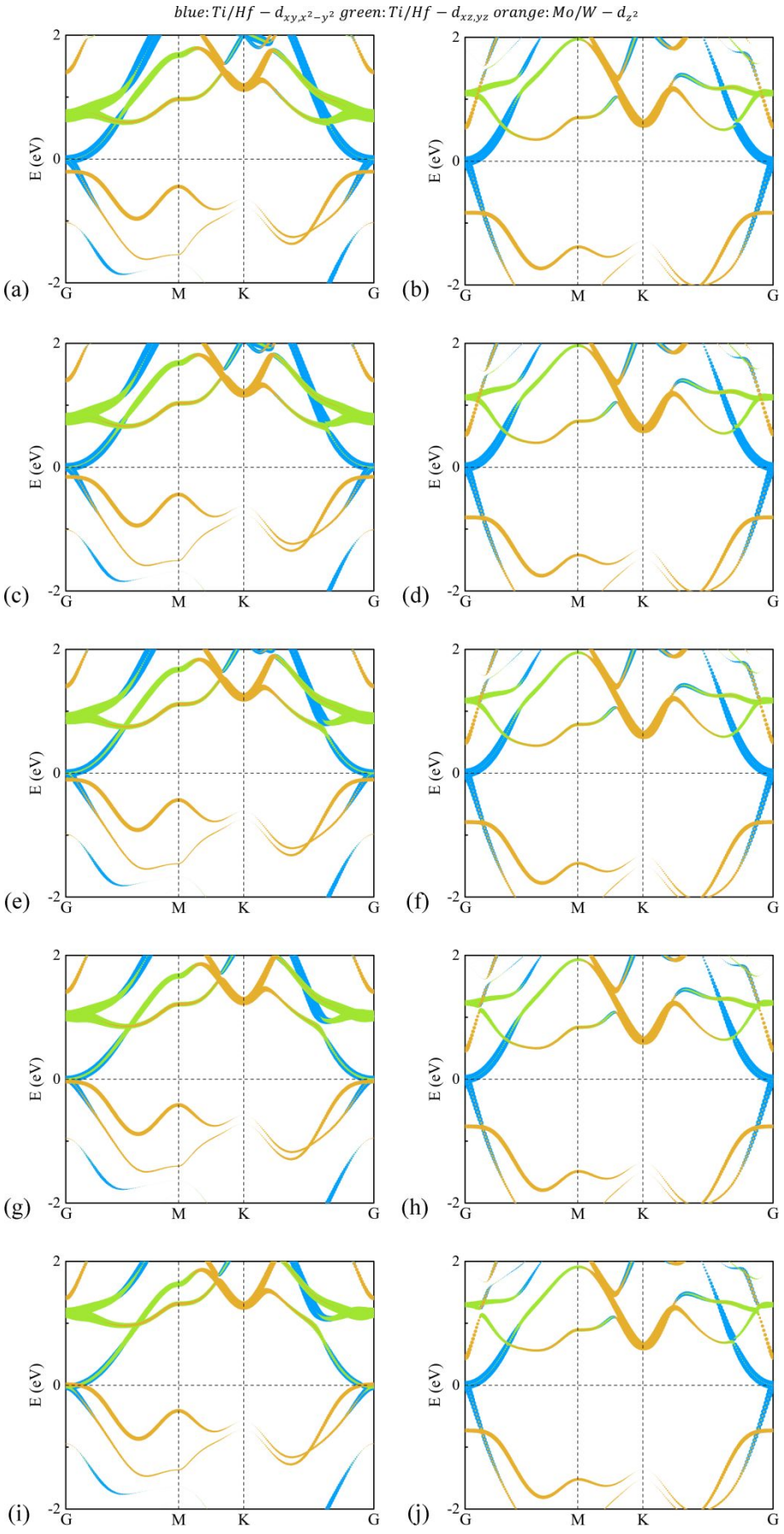
blue: Ti/Hf − d_{xy,x²−y²} green: Ti/Hf − d_{xz,yz} orange: Mo/W − d_{z²}
(a)
(b)
(c)
(d)
(e)
(f)
(g)
(h)
(i)
(j)
E (eV)
2
0
-2
G
M
K
G

Figure S4. Projected band structures of $Mo_2TiC_2O_2$ in GGA + U, where (a) U = 0 eV, (c) U = 1 eV, (e) U = 2 eV, (g) U = 3 eV, and (i) U = 4 eV. Projected band structures of $W_2HfC_2O_2$ in GGA + U, where (b) U = 0 eV, (d) U = 1 eV, (f) U = 2 eV, (h) U = 3 eV, and (j) U = 4 eV. The Fermi level is set to zero energy.

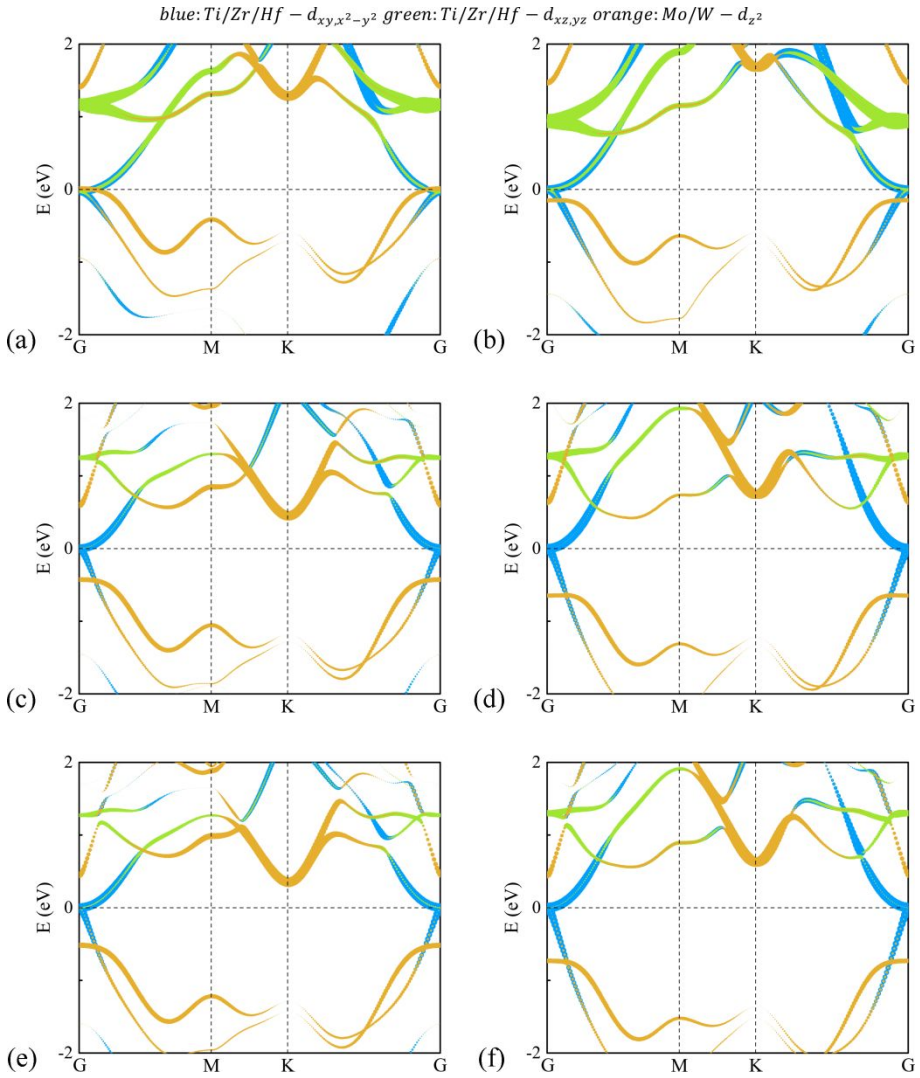

Figure S5. Projected band structures of (a) $Mo_2TiC_2O_2$, (b) $W_2TiC_2O_2$, (c) $Mo_2ZrC_2O_2$, (d) $W_2ZrC_2O_2$, (e) $Mo_2HfC_2O_2$, and (f) $W_2HfC_2O_2$ in GGA + U (U = 4 eV). The Fermi level is set to zero energy.

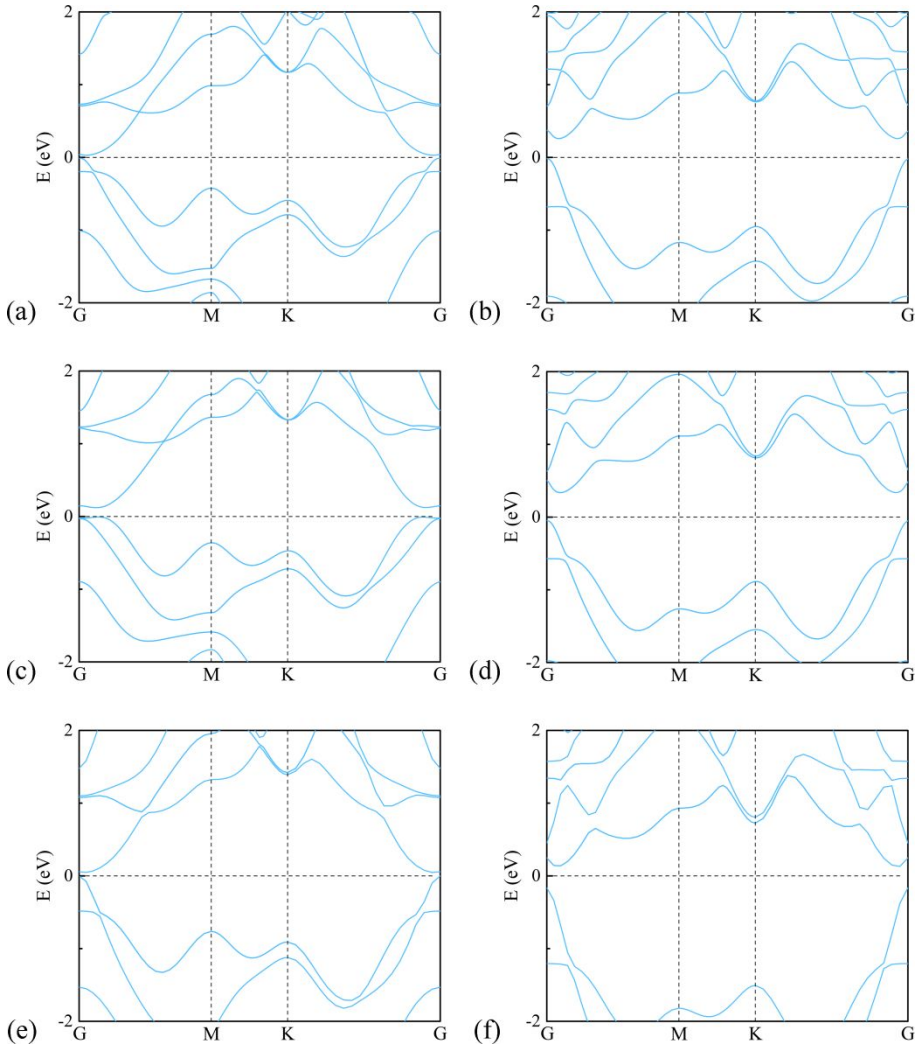

Figure S6. Electronic band structures of $Mo_2TiC_2O_2$ in (a) GGA, (c) GGA+ U (U = 4 eV), and (e) HSE. Electronic band structures of $W_2HfC_2O_2$ in (b) GGA, (d) GGA+ U (U = 4 eV), and (f) HSE. The SOC interaction is considered in the calculation of the band structures. The Fermi level is set to zero energy.

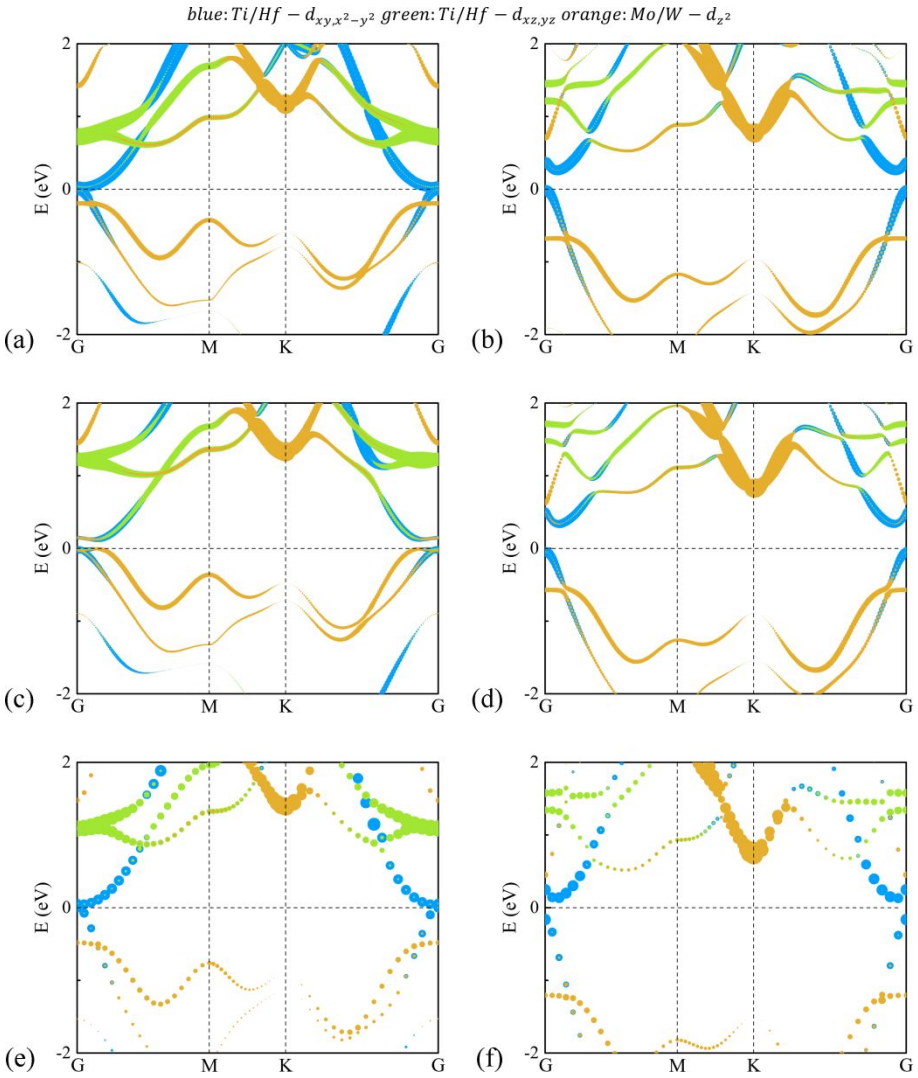

Figure S7. Projected band structures of $Mo_2TiC_2O_2$ in (a) GGA, (c) GGA+ *U* (*U* = 4 eV), and (e) HSE. Projected band structures of $W_2HfC_2O_2$ in (b) GGA, (d) GGA+ *U* (*U* = 4 eV), and (f) HSE. The SOC interaction is considered in the calculation of the band structures. The Fermi level is set to zero energy.

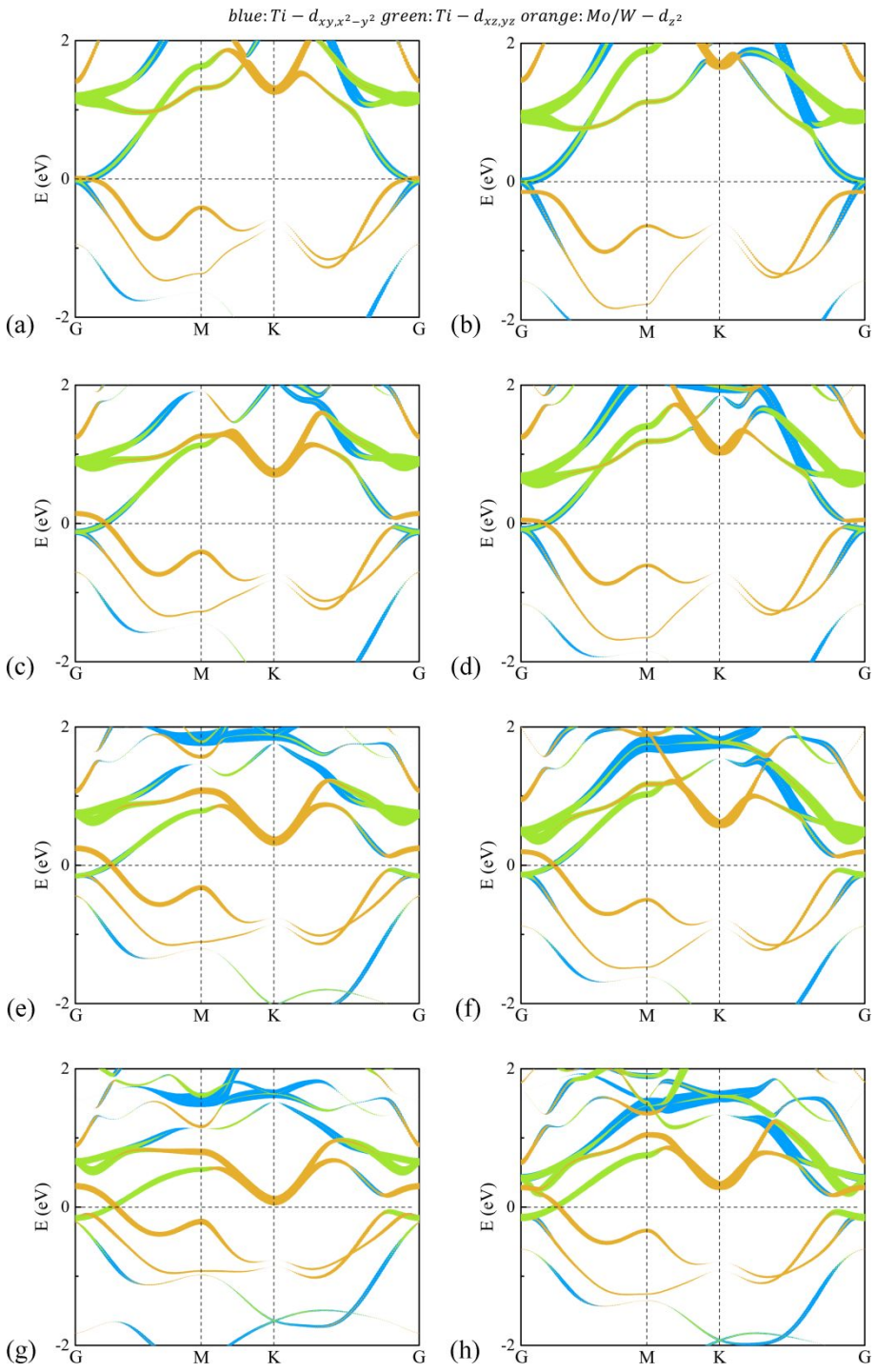

Figure S8. Projected band structures of $Mo_2TiC_2O_2$ (a) in equilibrium, (c) at strain $\varepsilon = 5\%$, (e) at strain $\varepsilon = 10\%$, and (g) at strain $\varepsilon = 15\%$. Projected band structures of $W_2TiC_2O_2$ (b) in equilibrium, (d) at strain $\varepsilon = 5\%$, (f) at strain $\varepsilon = 10\%$, and (h) at strain $\varepsilon = 15\%$. The Fermi level is set to zero energy.

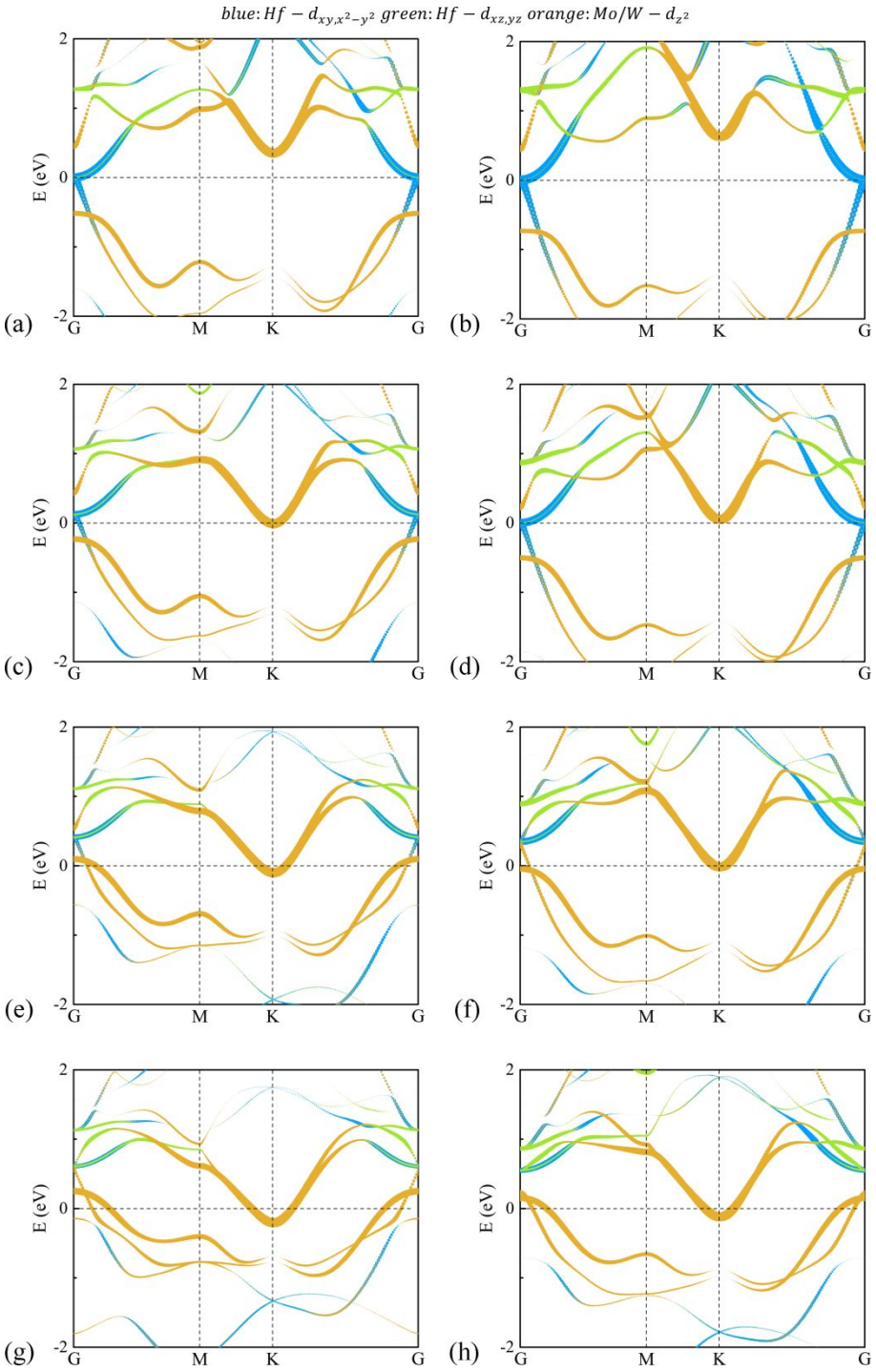

Figure S9. Projected band structures of $Mo_2HfC_2O_2$ (a) in equilibrium, (c) at strain ε = 5%, (e) at strain ε = 10%, and (g) at strain ε = 15%. Projected band structures of $W_2HfC_2O_2$ (b) in equilibrium, (d) at strain ε = 5%, (f) at strain ε = 10%, and (h) at strain ε = 15%. The Fermi level is set to zero energy.

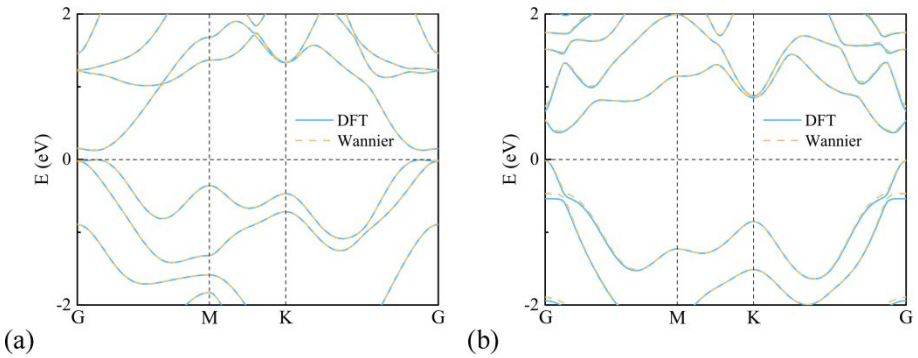

Figure S10. The fitted band structures to DFT and MLWFs for (a) $Mo_2TiC_2O_2$ and (b) $W_2HfC_2O_2$.

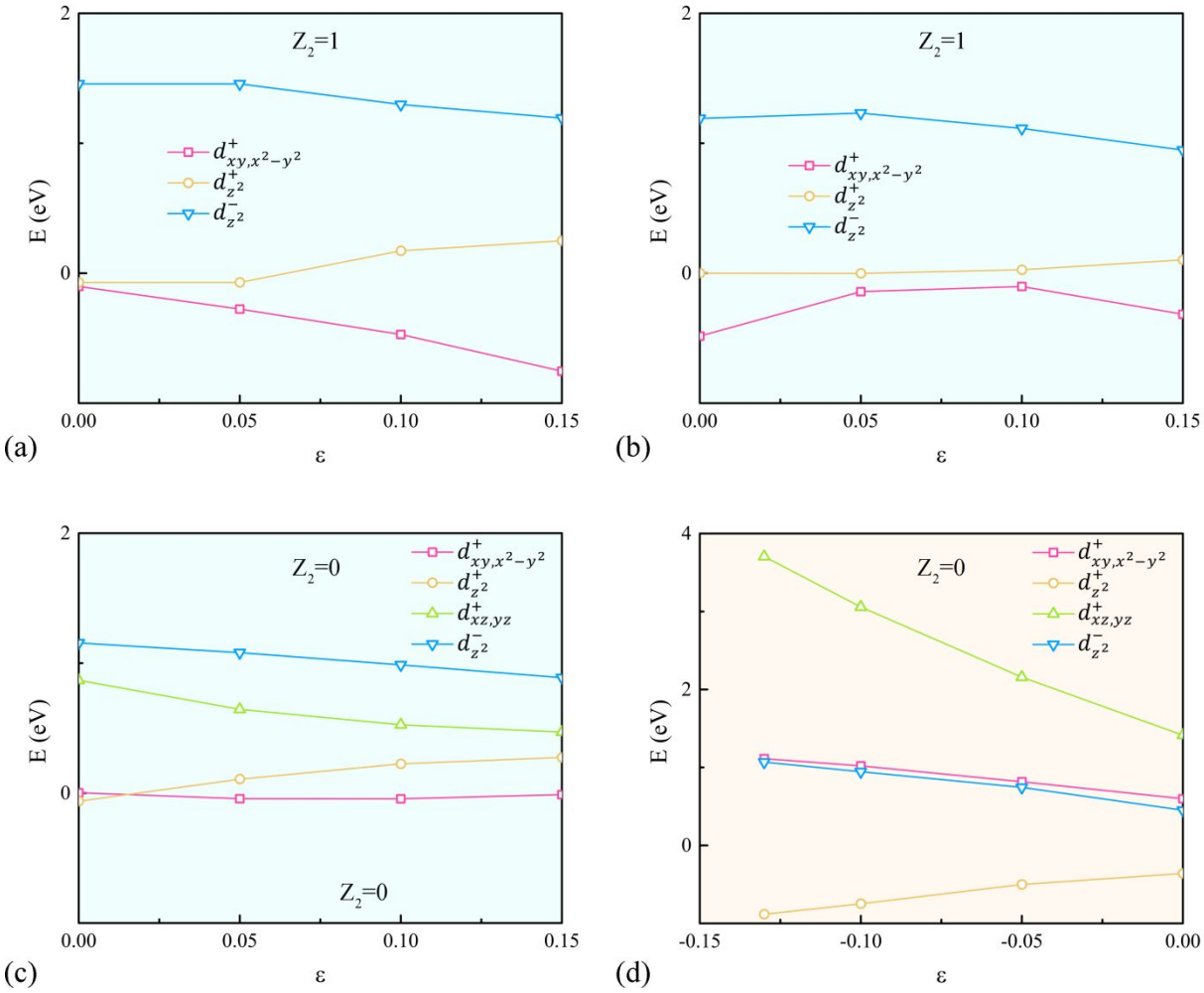

Figure S11. Energy levels of $|M'' - d_{z^2}^{\pm}\rangle$, $|M'' - d_{xy,x^2-y^2}^{+}\rangle$, and $|M'' - d_{z^2}^{-}\rangle$ states at Γ point vs strain ε curves of (a) Mo_2CO_2 and (b) W_2CO_2. Energy levels of $|M'' - d_{z^2}^{\pm}\rangle$, $|M' - d_{xy,x^2-y^2}^{+}\rangle$, $|M' - d_{xz,yz}^{+}\rangle$ and $|M'' - d_{z^2}^{-}\rangle$ states at Γ point vs strain ε curves of (c) $Mo_2Ti_2C_3O_2$ and (d) $W_2Hf_2C_3O_2$. Note that a compression strain is adopted in $W_2Hf_2C_3O_2$, different from the tensile strain in the others.

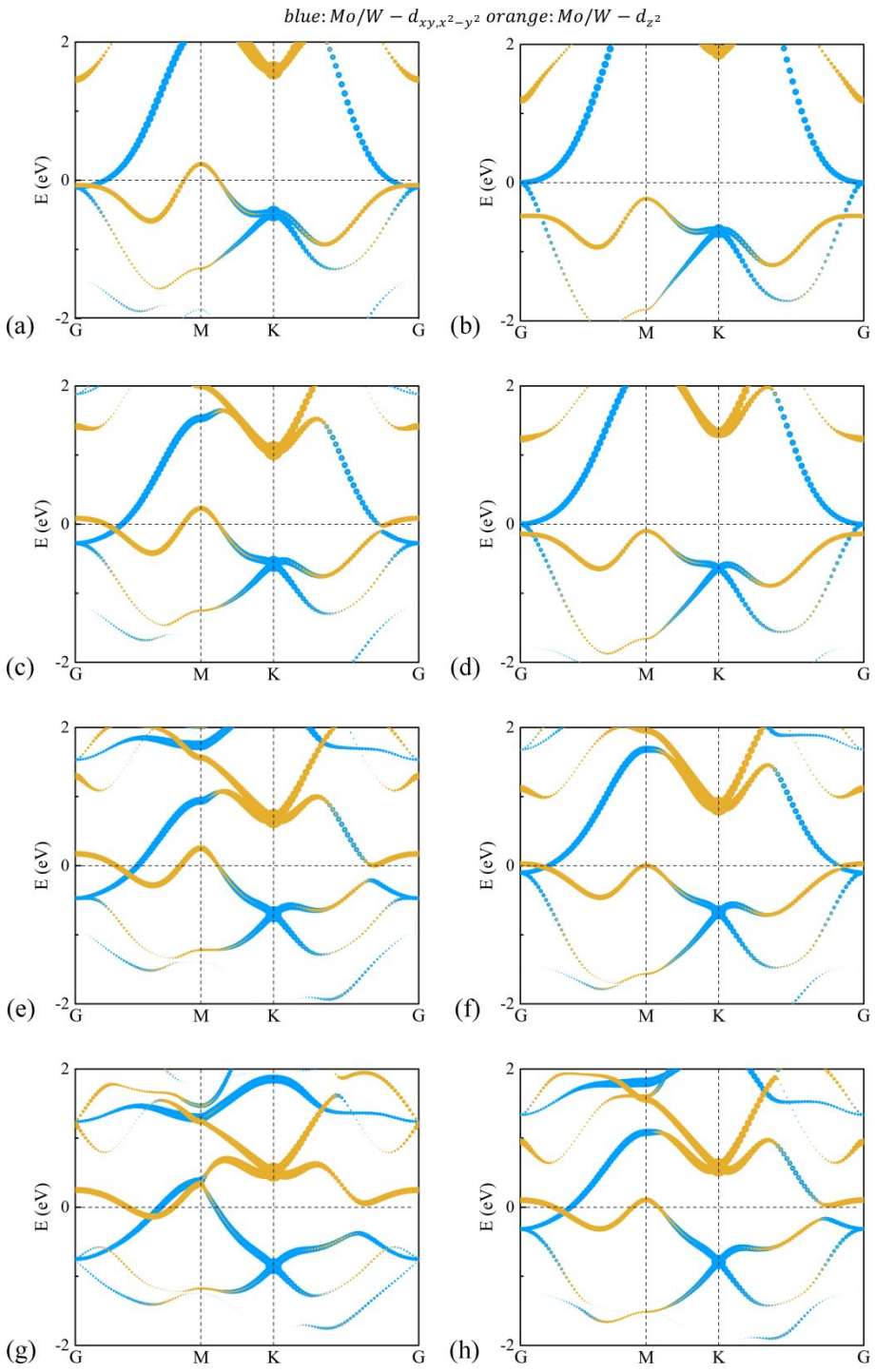

Figure S12. Projected band structures of Mo_2CO_2 (a) in equilibrium, (c) at strain $\varepsilon = 5\%$, (e) at strain $\varepsilon = 10\%$, and (g) at strain $\varepsilon = 15\%$. Projected band structures of W_2CO_2 (b) in equilibrium, (d) at strain $\varepsilon = 5\%$, (f) at strain $\varepsilon = 10\%$, and (h) at strain $\varepsilon = 15\%$. The Fermi level is set to zero energy.

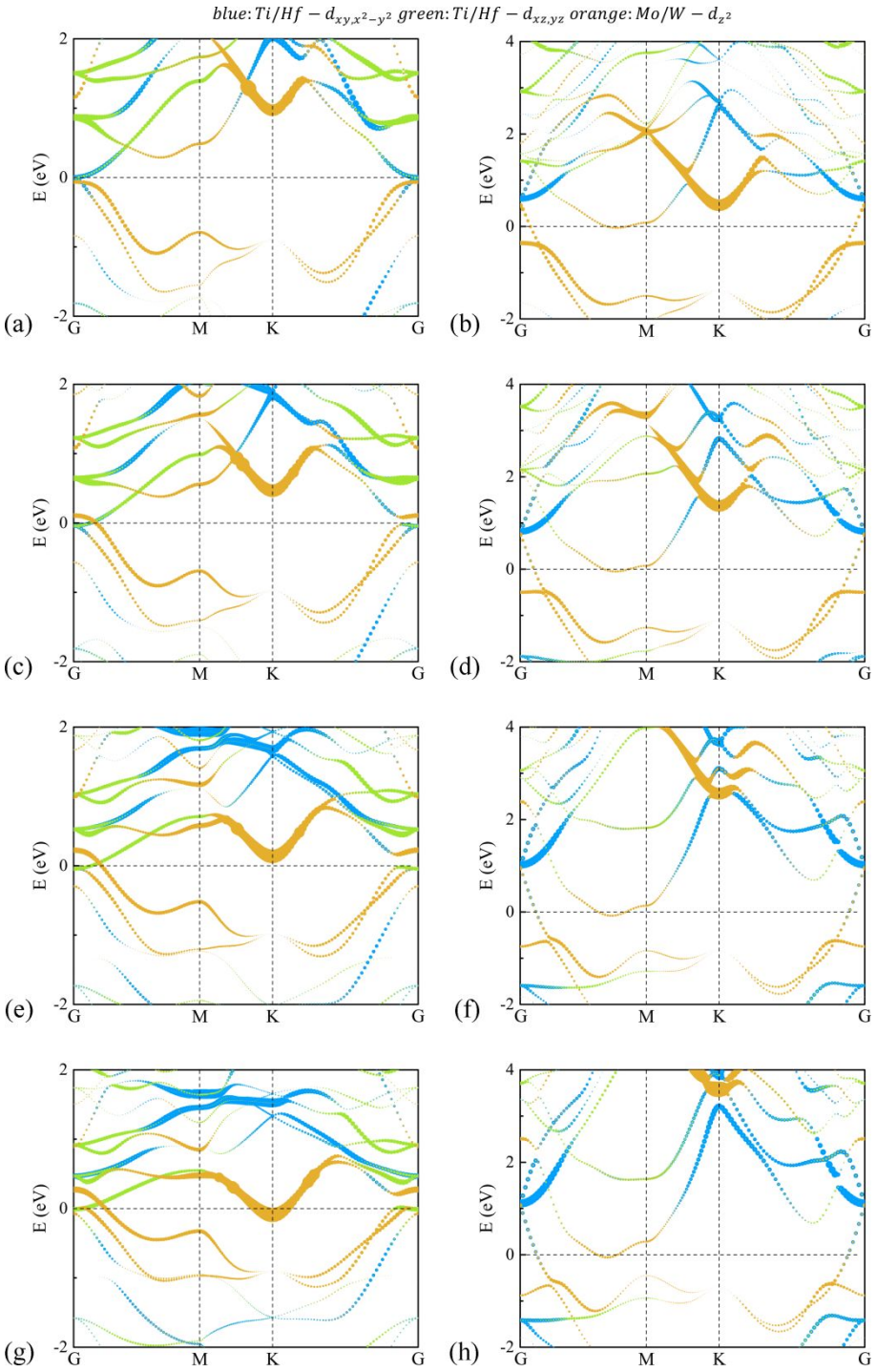

Figure S13. Projected band structures of $Mo_2Ti_2C_3O_2$ (a) in equilibrium, (c) at strain ε = 5%, (e) at strain ε = 10%, and (g) at strain ε = 15%. Projected band structures of $W_2Hf_2C_3O_2$ (b) in equilibrium, (d) at strain ε = -5%, (f) at strain ε = -10%, and (h) at strain ε = -15% (the symbol "-" represents the compression strain). The Fermi level is set to zero energy.

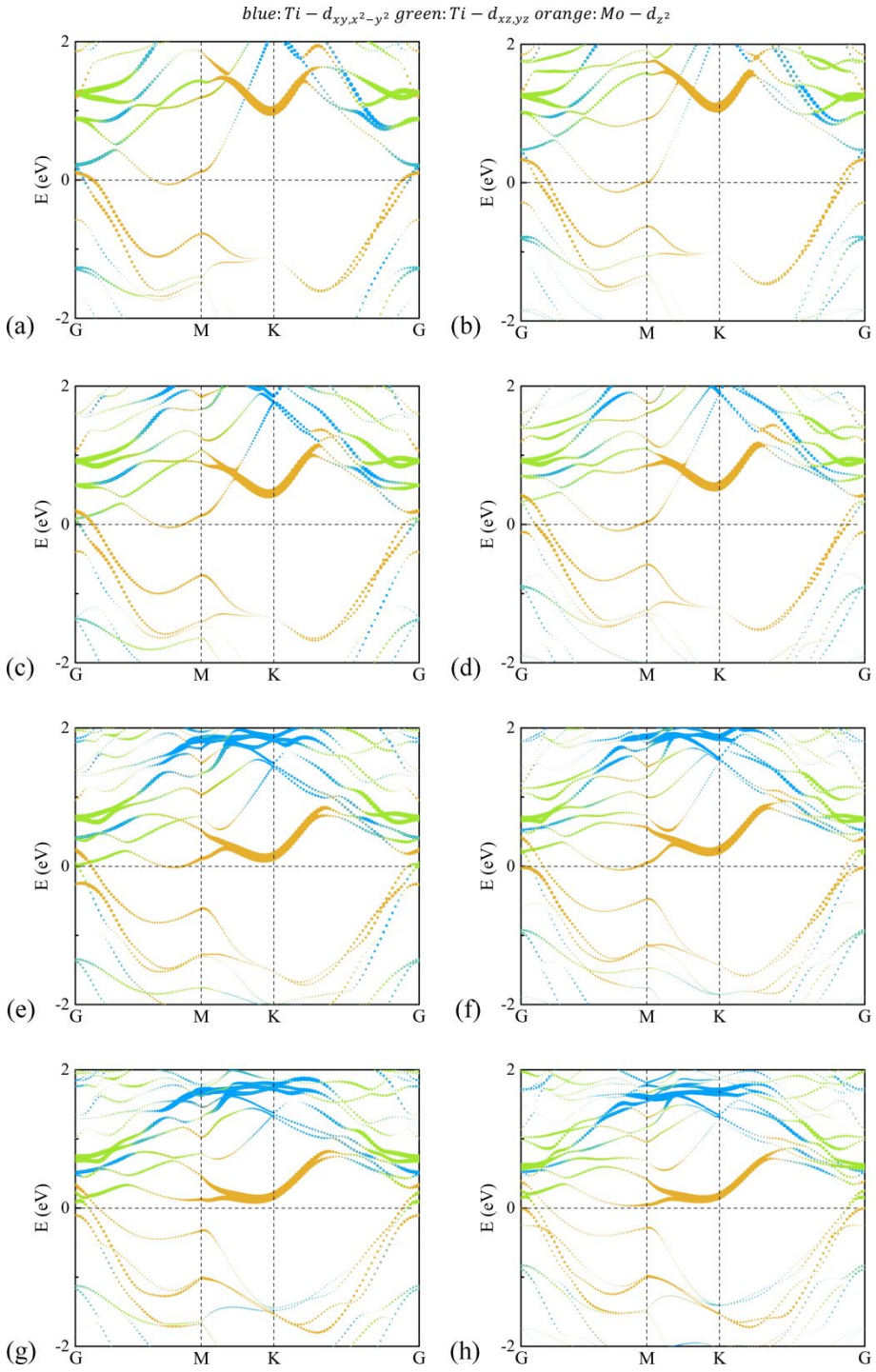

Figure S14. Projected band structures of $Mo_2Ti_3C_4O_2$ (a) in equilibrium, (c) at strain ε = 5%, (e) at strain ε = 10%, and (g) at strain ε = 15%. Projected band structures of $Mo_2Ti_4C_5O_2$ (b) in equilibrium, (d) at strain ε = 5%, (f) at strain ε = 10%, and (h) at strain ε = 15%. The Fermi level is set to zero energy.

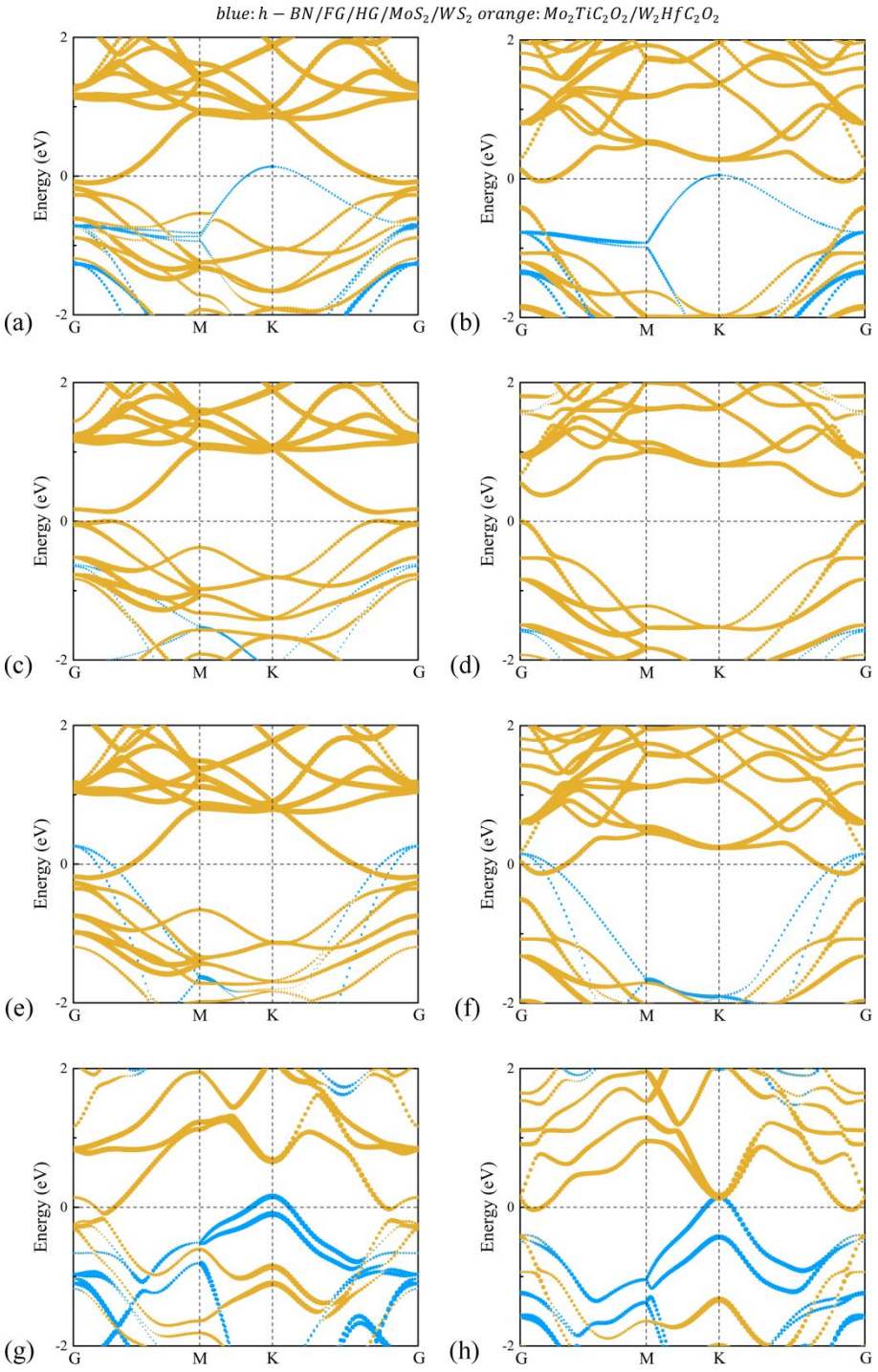

Figure S15. Atomic projected band structures of $Mo_2TiC_2O_2$ with large-gap coating layer (a) h-BN, (c) fluorographene, (e) graphane, (g) MoS_2. Atomic projected band structures of $W_2HfC_2O_2$ with large-gap coating layer (b) h-BN, (d) fluorographene, (f) graphane, (h) WS_2. The Fermi level is set to zero energy.

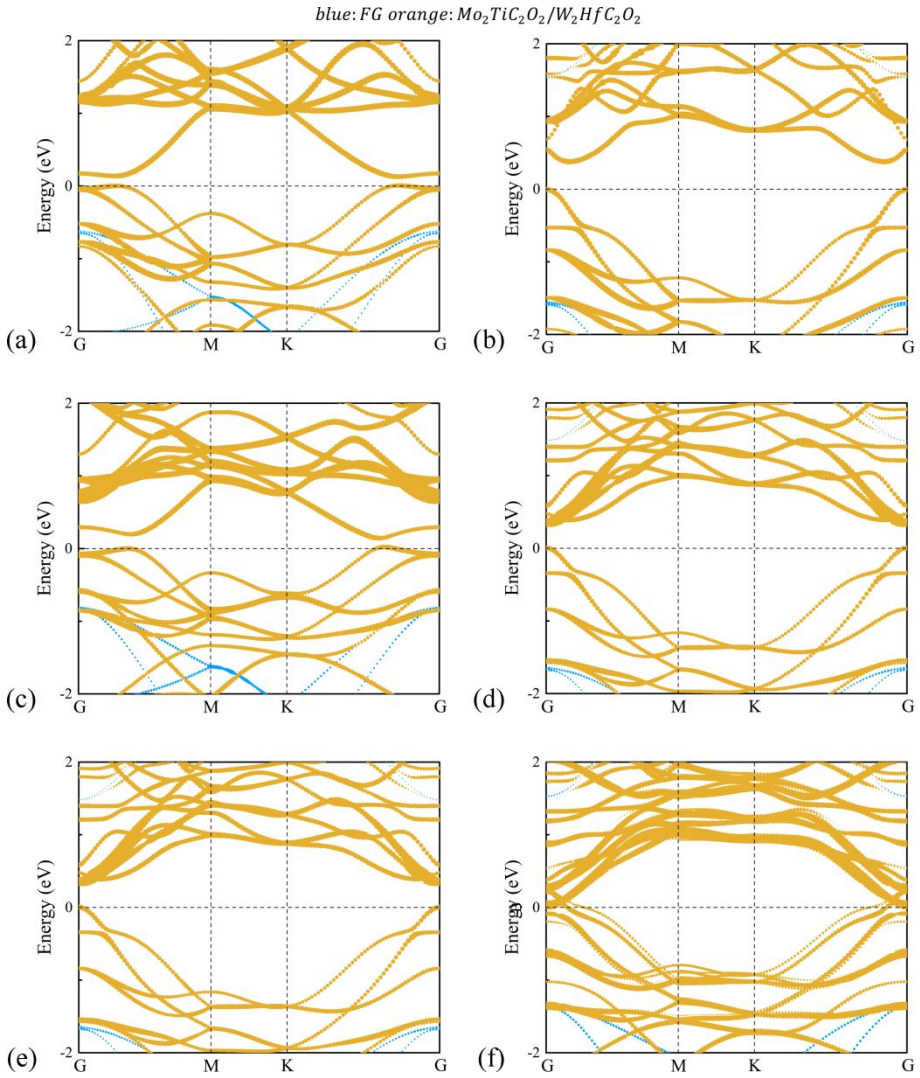

Figure S16. Atomic projected band structures of $Mo_2TiC_2O_2$ with large-gap coating layer fluorographene (a) in equilibrium, (c) at strain ε = 5%, and (e) at strain ε = 10%. Atomic projected band structures of $W_2HfC_2O_2$ with large-gap coating layer fluorographene (b) in equilibrium, (d) at strain ε = 5%, and (f) at strain ε = 10%. The Fermi level is set to zero energy.